



**HAL**  
open science

**Last glacial fire regime variability in western France  
inferred from microcharcoal preserved in core  
MD04-2845, Bay of Biscay**

Anne-Laure Daniau, Maria Fernanda Sánchez Goñi, Josette Duprat

► **To cite this version:**

Anne-Laure Daniau, Maria Fernanda Sánchez Goñi, Josette Duprat. Last glacial fire regime variability in western France inferred from microcharcoal preserved in core MD04-2845, Bay of Biscay. *Quaternary Research*, 2009, 71 (3), pp.385-396. 10.1016/j.yqres.2009.01.007 . hal-03210043

**HAL Id: hal-03210043**

**<https://hal.science/hal-03210043>**

Submitted on 27 Apr 2021

**HAL** is a multi-disciplinary open access archive for the deposit and dissemination of scientific research documents, whether they are published or not. The documents may come from teaching and research institutions in France or abroad, or from public or private research centers.

L'archive ouverte pluridisciplinaire **HAL**, est destinée au dépôt et à la diffusion de documents scientifiques de niveau recherche, publiés ou non, émanant des établissements d'enseignement et de recherche français ou étrangers, des laboratoires publics ou privés.



Contents lists available at ScienceDirect

## Quaternary Research

journal homepage: [www.elsevier.com/locate/yqres](http://www.elsevier.com/locate/yqres)

# Last glacial fire regime variability in western France inferred from microcharcoal preserved in core MD04-2845, Bay of Biscay

Anne-Laure Daniau<sup>a,b,\*</sup>, Maria Fernanda Sánchez Goñi<sup>a</sup>, Josette Duprat<sup>a</sup>

<sup>a</sup> Université de Bordeaux1, EPHE, CNRS UMR5805, EPOC, bât B18, Avenue des Facultés, 33405 TALENCE Cedex, France

<sup>b</sup> Université de Bordeaux1, CNRS UMR5199 PACEA, Institut de Préhistoire et Géologie du Quaternaire, bât B18, Avenue des Facultés, 33405 TALENCE Cedex, France

## ARTICLE INFO

**Article history:**  
Received 17 January 2008  
Available online xxx

**Keywords:**  
Marine sequence  
Charcoal  
Biomass burning  
France  
Dansgaard–Oeschger events  
Heinrich events

## ABSTRACT

High resolution multiproxy analysis (microcharcoal, pollen, organic carbon, *Neogloboquadrina pachyderma* (s), ice rafted debris) of the deep-sea record MD04-2845 (Bay of Biscay) provides new insights for understanding mechanisms of fire regime variability of the last glacial period in western France. Fire regime of western France closely follows Dansgaard–Oeschger climatic variability and presents the same pattern than that of southwestern Iberia, namely low fire regime associated with open vegetation during stadials including Heinrich events, and high fire regime associated with open forest during interstadials. This supports a regional climatic control on fire regime for western Europe through fuel availability for the last glacial period. Additionally, each of Heinrich events 6, 5 and 4 is characterised by three episodes of fire regime, with a high regime bracketed by lower fire regime episodes, related to vegetational succession and complex environmental condition changes.

© 2009 University of Washington. All rights reserved.

## Introduction

Beyond man-made fires, biomass burning depends on climate and also appears to be a significant driver for climate change through the release of greenhouse gases, namely carbon dioxide, methane, nitric oxide and aerosols (Crutzen et al., 1979; Lobert et al., 1990; Andreae and Merlet, 2001; van Aardenne et al., 2001; Van der Werf et al., 2004; Thonicke et al., 2005). Variations of atmospheric greenhouse gas concentration in concert with the millennial-scale Dansgaard–Oeschger (D–O) climatic variability have been identified in Greenland and Antarctic ice cores (Petit et al., 1999; Flückiger et al., 2004). However, the influence of fire regime (fire intensity, severity, size, frequency at regional and centuries time-scale following Hu et al., 2006) on these variations is poorly understood due to the lack of high-resolution fire regime records covering this period. A recent synthesis of charcoal records covering the last 21 ka (Power et al., 2007) shows that spatial fire regime variations were not constant through this time related to changes of climate and local fuel load. High resolution deep-sea microcharcoal records covering the last glacial period (LGP) can provide new perspectives for understanding mechanisms of fire regime variability such as vegetation type, amount of fuel, climate changes through periods of drought, lightning storm position, human activity or orbital forcing.

The impact of D–O climatic variability on fire regime was detected for the first time in southwestern Iberia (Daniau et al., 2007), a region that experiences at present a frequent fire activity. The Iberian fire regime variability has been related to changes of fuel amount through shifts in vegetation between Greenland stadials (GS) including Heinrich events (HE), which experienced low fire regime associated with semi-desert vegetation, and Greenland interstadials (GI), which experienced high fire regime associated with open Mediterranean forest and heathland development. Changes in moisture and temperature conditions determine the type of vegetation, which in turn controls the amount of fuel and the fire return interval.

Fire regime and vegetation shift registered in southwestern Iberia between GS and GI have been related to prevailing atmospheric situations similar to the present-day positive and negative North Atlantic Oscillation (NAO) index, respectively (Daniau et al., 2007). The NAO is one of the major mechanisms responsible for the present-day wintertime temperature and precipitation patterns across the North Atlantic region. During the positive phase of NAO, the Mediterranean region experiences major drought because of the shift of the westerlies northwards, whereas a negative phase brings humidity to this region due to the weakening and southward displacement of westerlies to mid-latitudes. Winter moisture variation in southwestern France is, as in Iberia, negatively correlated to the NAO (Trigo et al., 2002). While a NAO-like pattern has been proposed to explain fuel availability and therefore fire regime during GS and GI in southwestern Iberia, we still do not know whether this atmospheric mechanism was at hand in regions located further north.

This work has two main objectives: a) to document for the first time the fire regime of western France during the LGP, and b) to

\* Corresponding author. Université de Bordeaux1, CNRS UMR5199 PACEA, Institut de Préhistoire et Géologie du Quaternaire, bât B18, Avenue des Facultés, 33405 TALENCE Cedex, France. Fax: +33 5 40 00 84 51.

E-mail addresses: [al.daniau@ipgq.u-bordeaux1.fr](mailto:al.daniau@ipgq.u-bordeaux1.fr) (A.-L. Daniau), [mf.sanchezgoni@epoc.u-bordeaux1.fr](mailto:mf.sanchezgoni@epoc.u-bordeaux1.fr) (M.F.S. Goñi), [jm.duprat@orange.fr](mailto:jm.duprat@orange.fr) (J. Duprat).

74 examine whether the fuel amount is, as in southwestern Iberia, the  
 75 main factor controlling the millennial-scale fire regime variability in  
 76 this region. For this, we analysed microcharcoal particles preserved in  
 77 deep-sea core MD04-2845 in the Bay of Biscay at the latitude of  
 78 Bordeaux. Complementary analysis of organic carbon on this core has  
 79 been carried out in order to understand better the microcharcoal  
 80 signal. Preliminary  $\delta^{18}\text{O}$  isotopic measurements and previous studies  
 81 of this core (carbonates, ice rafted debris, planktonic foraminifera,  
 82 pollen) have shown that it covers Marine Isotope Stage (MIS) 7 to 1  
 83 and revealed the impact of D–O climatic variability and Heinrich  
 84 events in the ocean and on land (Sánchez Goñi et al., 2008). The direct  
 85 correlation between past fire regime and these climatic proxies, in  
 86 particular vegetation shifts, allows the discussion of the complex  
 87 relationships between fire and climate.

## 88 Environmental setting

### 89 Present-day vegetation, fire and climate

90 Western France extends from 42°N to 48°N (Fig. 1) and comprises  
 91 essentially the Loire–Britany and the Adour–Garonne river basins. This  
 92 region is characterised by a temperate and oceanic climate. Winter  
 93 precipitation in its southern part is particularly influenced by the NAO  
 94 (Trigo et al., 2002; Dupuis et al., 2006). Annual precipitation of  
 95 the Loire–Britany basin is 500–700 mm and 600–1000 mm for the Adour–  
 96 Garonne basin. The specific region covered by mountains (the Massif  
 97 Central and the Pyrenean) receive more than 1500 mm. The mean  
 98 temperatures in winter vary from 0 to more than 8°C on the Atlantic  
 99 coast, and from 15 to more than 22°C in summer (Serryn, 1994). The  
 100 region is colonised today by Atlantic vegetation (Fig. 1) characterised

by deciduous forests (mainly oaks, ash, beech, birch) and coniferous  
 trees restricted to montane and some southern maritime areas, and by  
 semi-natural grasslands (Polunin and Walters, 1985). 103

104 Compared to Spain, Portugal, Italy and Greece, France does not  
 105 experience a high fire activity. The average of 30,738 ha of burnt  
 106 wooded area and 5218 forest fires for the period AD 1980–2000  
 107 represent only 4% and 10%, respectively, of that of the other countries  
 108 (European Commission, 2001). Fire activity in France is mainly  
 109 concentrated in its Mediterranean part, during summer months  
 110 (July and August). The western part of France is, on the whole, not  
 111 affected by large fires, but local fires caused by lightning do occur  
 112 (<http://www.feudeforet.org/>). However, as the present-day incidence  
 113 and spatial distribution of fires resulting from lightning strikes is  
 114 restricted by human activities, this type of ignition may have been  
 115 more important in the past.

### Oceanic surface circulation and wind patterns 116

117 The current circulation pattern in the Bay of Biscay (Fig. 2) is  
 118 characterised by a mean southward surface circulation during  
 119 summer, the formation of eddies near the shelf break and a weak  
 120 flow of the slope current. During winter, the mean surface circulation  
 121 is dominated by a strong poleward intrusion of the slope current along  
 122 the Iberian Peninsula and the Armorican and Celtic slopes, with a  
 123 branch of westward orientation inside the Bay of Biscay, generating a  
 124 particular cyclonic cell circulation centred at 46°N, 6.5°W (Durrieu de  
 125 Madron et al., 1999; Colas, 2003). This poleward slope current (the  
 126 Navidad current) in the winter season brings warm surface water into  
 127 the Bay of Biscay and may affect biological productivity (Garcia-Soto et  
 128 al., 2002). Its strength depends on the wind pattern over the Bay

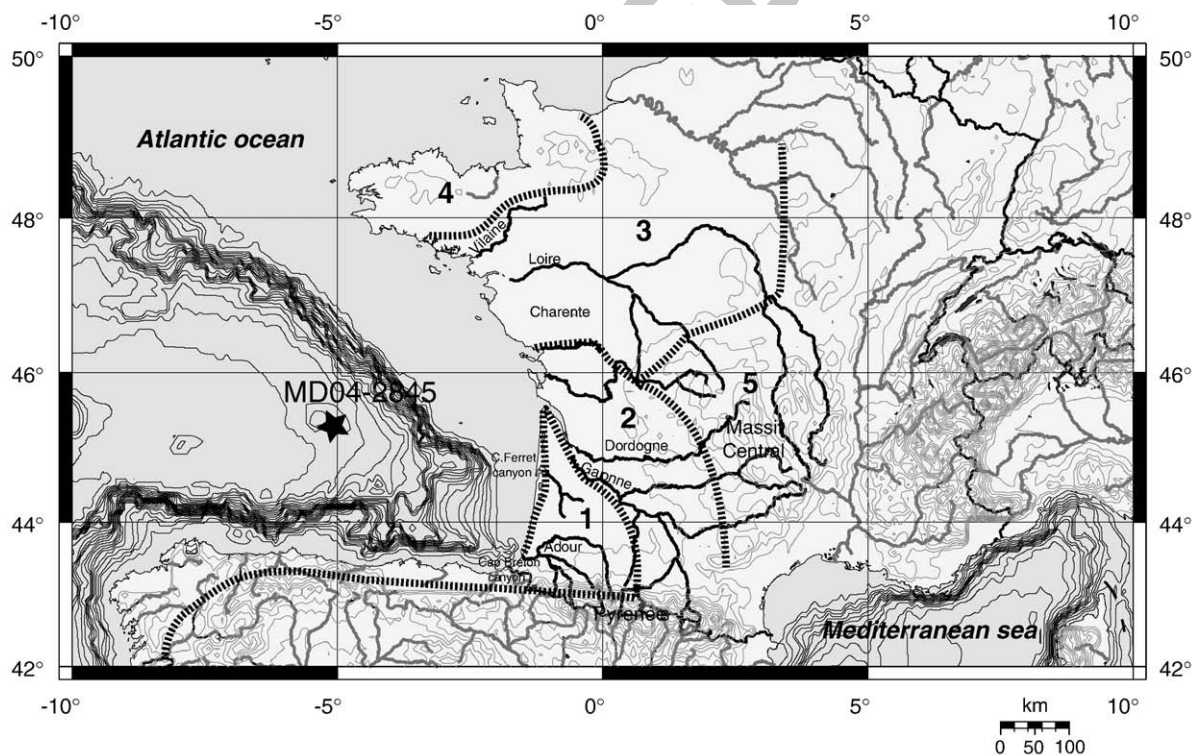


**Figure 1.** Map of France showing the location of core MD04-2845 (filled star). Black dotted lines represent the division of the Atlantic and Sub-atlantic vegetation domains simplified from Ozenda (1982). Area 1; Southwestern France is characterised by vegetation composed of *Quercus robur*, *Q. pyrenaica*, *Castanea sativa*, *Pinus pinaster* with some *Q. suber*. Area 2; This region presents a mosaic of *Quercus pubescens*, *Q. robur* and *Q. petraea*. Some *Q. ilex* is found near the coast. Area 3; Vegetation of the central-western part of France is mainly characterised by a mosaic of *Q. robur* on alluvial soils and *Q. petraea* associated with hornbeam (*Carpinus betulus*) on slope and drained areas. Area 4; Vegetation of the north-western part, characterised by a high level of precipitation, is a mosaic of three main floristic associations including *Fagus* forest, *Fagus-Quercus robur* forest and heathland community dominated by *Calluna* and *Ulex*. Near the coast, *Fagus* forest is replaced by *Quercus-Praxinus* forest. Area 5; The Massif Central is colonised mainly by *Q. robur*, *Q. petraea*, *Q. pubescens* and *Castanea sativa* between 600 and 800 m. *Fagus*, *Fagus-Pinus* forest, heathland, *Ulex*, and *Pinus sylvestris* forest are found above. Between 1500 and 1600 m the vegetation is composed of heathland of *Calluna* and *Juniperus sibirica*.

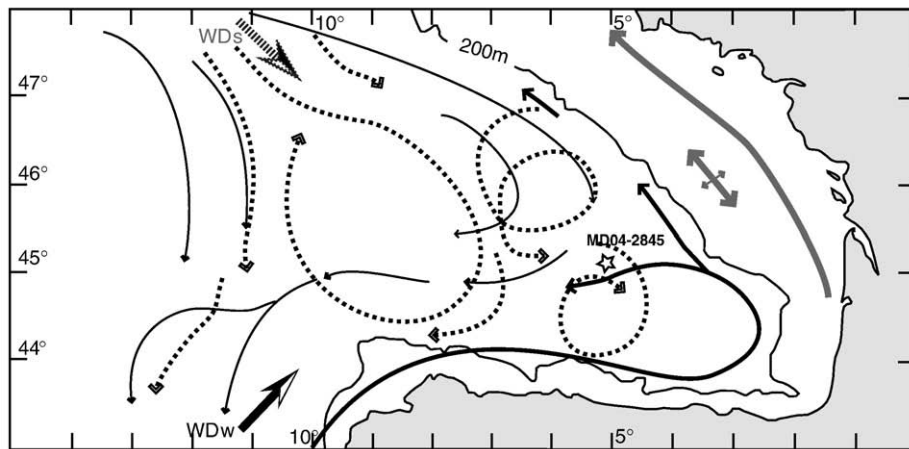


**Figure 2.** Map of oceanic circulation and wind directions in the Bay of Biscay during summer and winter situations (modified from Durrieu de Madron et al., 1999 and Koutsikopoulos and Le Cann, 1996). Below 200 m depth, oceanic circulation during winter is represented by black lines (with a strong poleward of the slope current corresponding to the Navidad current). Black dotted lines represent oceanic circulation during summer. Shelf residual current (along the coast) and wind induced currents (grey double arrows) are found on the shelf. Arrows represent dominant wind directions. WD w (black arrow): wind direction in winter. WD s (grey dotted arrow): wind direction in summer.

related to the NAO, with a low NAO index leading to an intensified Navidad current (García-Soto et al., 2002).

The mean wind direction over the Bay (Fig. 1) is from northwest in summer and from southwest in the winter season. However, a southward direction towards northern Iberia prevailed inside the bay for both situations (Colas, 2003). Upwellings appear during spring and summer period along the shelf area in relation to wind blowing to the coast (Heaps, 1980). Northwesternly to northerly wind events create coastal upwellings off southern Brittany, Vendée and Landes. Westerly winds generate upwelling to the north of the Loire (Froidefond et al., 1996; Lazare and Jégou, 1998; Puillat et al., 2004). Core MD04-2845 is outside of these upwelling areas.

#### Morphology and recent sedimentation

The Bay of Biscay is characterised by a continental shelf oriented NW–SE along the French coast and E–W along the Spanish coast, with a platform relatively flat. Its large width along the French coast prevents direct feeding on the shelf break by bottom nepheloid layers (Jouanneau et al., 1999) except for the region of the Cap-Ferret Canyon (Ruch et al., 1993). Two sedimentary systems characterise the continental shelf of this bay, an inner shelf (<100–120 m) and an outer shelf (>120 m) showing a general grain-size fining southward (Allen and Castaing, 1977). Pre- and early Holocene offshore mud and sands occupy the zone between 75 and 120 m depth, and coarse sands and gravels carried by rivers between 30–75 m, probably related to the influence of the Gironde paleoriver detected 50 km seaward of the estuary mouth (Lericolais et al., 2001).

Rivers (Fig. 1) are the main sources of fine sediments (including microcharcoal and pollen) to the Bay of Biscay, taking into account that westerlies are the dominant winds in the Bay. The main rivers, the Garonne and the Dordogne feeding the Gironde estuary, the Loire, the Vilaine, the Charente and the Adour rivers, deliver about  $2.5 \times 10^6 \text{ t yr}^{-1}$  of continental fine sediments, with the Gironde estuary accounting for 60% of this amount (Jouanneau et al., 1999). The continental suspended matter which spreads out from the Gironde estuary on the shelf is transported to the north along the coast by a surface turbid plume (Castaing, 1981) and may be carried to the Cap-Ferret Canyon in a bottom nepheloid layer (Ruch et al., 1993). However, an estimated  $0.9 \times 10^6 \text{ t yr}^{-1}$  of fine sediments could reach the slope and eventually the open ocean (Jouanneau et al., 1999).

Experimental studies on the present-day pollen–vegetation relationship confirms that marine pollen assemblages from the south-

western French margin represent an integrated image of the regional vegetation, including coastal, low and high altitude areas (Turon, 1984). Pollen assemblages preserved in core MD04-2845 therefore reflect the vegetation colonising both hydrographic basins with headwaters located in the Massif Central and the Pyrenees, respectively.

#### Materials and methods

##### Core location, sampling and chronostratigraphy

Deep-sea core MD04-2845 (45°21'N, 5°13'W; 4175 m water depth) (Fig. 1) was collected during the Alienor cruise in 2004 in the Bay of Biscay using the CALYPSO Kullenberg corer aboard the Marion Dufresne vessel. The site is located 350 km from the nearest coastline on the Gascogne Seamount, without influence of turbidite currents. The sediments are mainly composed of clayey mud with sparse silty laminations, with 10–65% carbonate. Observations of X-ray analysis using SCOPIX image-processing have shown a well preserved sedimentary sequence not perturbed by turbidites in the analysed part of core MD04-2845 between 760 and 2245 cm depth. A sedimentary hiatus appears between 1714 and 1740 cm depths.

Carbonate content measurements and onboard sediment reflectivity curve along with IRD counting, polar foraminifer *Neogloboquadrina pachyderma* (s) percentages and foraminifer assemblage-derived sea surface temperatures (SST) of core MD04-2845 define the last interglacial, D–O events and Heinrich events. To compare fire regime of western France with that recorded in southwestern Iberia (Daniau et al., 2007), the age model of the marine core MD04-2845 is based on that of the southern Iberian margin core MD95-2042 (37°14'N, 10°11'W), which is AMS  $^{14}\text{C}$  dated and calibrated to GISP2 and GRIPSS09sea chronologies, assuming that changes in the polar front position were synchronous in the North Atlantic region (Shackleton et al., 2000, 2004; Bard et al., 2004). Control points used for the glacial interval of core MD04-2845 are derived from the correlation of the onset of GI and boundaries of HE detected in this core with those identified in core MD95-2042 (see synthesised table in Sánchez Goñi et al., 2008).

For the interval 680–892 cm (Table 1), we add 4 control points derived from the age model of the Iberian core used in Daniau et al. (2007). Ages of these control points are in good agreement with linear age model obtained from 10 AMS  $^{14}\text{C}$  ages obtained for core MD04-

**Table 1**  
Chronostratigraphic model for core MD04-2845

Lab code/event	Core depth (m)	Material	Conv. AMS <sup>14</sup> C age kyr (–400 yr)	Error yr ±	95.4% (2σ) Cal BP age ranges	( <sup>1</sup> ) Cal BP age (ka) median probability	( <sup>2</sup> ) Bard et al. (2004) age (ka)	( <sup>3</sup> ) Control points (ka) based on MD95-2042 chronology
SacA-002960	5.2	<i>G. bulloides</i>	16.890	150	19.782:20.365	20.03		
HE2/GIS2	6.8							23.95
SacA-002961	6.9	<i>N. pachyderma</i> (s)	20.420	140	24.016:24.890	24.44		
SacA-002962	7.1	<i>N. pachyderma</i> (s)	20.710	140	24.426:25.405	24.88		
SacA-002963	7.7	<i>N. pachyderma</i> (s)	21.860	160			25.82	
SacA-002964	7.9	<i>N. pachyderma</i> (s)	22.150	170			26.14	
Base HE2	8.1							26.25
SacA-002965	8.5	<i>G. bulloides</i>	24.050	210			28.22	
Onset GIS3	8.5							27.84
SacA-002966	8.6 <sup>a</sup>	<i>N. pachyderma</i> (s)	24.680 <sup>a</sup>	230			28.89 <sup>a</sup>	
SacA-002967	8.7 <sup>a</sup>	<i>N. pachyderma</i> (s)	24.630 <sup>a</sup>	230			28.84 <sup>a</sup>	
SacA-002968	8.9 <sup>a</sup>	<i>G. bulloides</i>	25.230 <sup>a</sup>	240			29.48 <sup>a</sup>	
HE3/GIS4	8.92							29.00
SacA-002969	9.0 <sup>a</sup>	<i>N. pachyderma</i> (s)	24.870 <sup>a</sup>	240			29.10 <sup>a</sup>	

A mean age (ka) has been calculated for consecutive levels (8.6–8.7 and 8.9–9 m) before applying linear interpolation to estimate age difference between control points (<sup>3</sup>) and ages based on calibrated AMS<sup>14</sup>C (<sup>1,2</sup>).

<sup>a</sup> Levels presenting small AMS<sup>14</sup>C inversions.

2845 in the interval HE3/GI4 to HE2/GI2 (mean age difference <400 yr). The samples presenting conventional AMS <sup>14</sup>C younger than 21,786 <sup>14</sup>C yr BP were calibrated by using CALIB Rev 5.0 program and “global” marine calibration data set (marine 04.14c) (Stuiver and Reimer, 1993; Hughen et al., 2004; Stuiver et al., 2005). <sup>14</sup>C radiometric ages older than 21,786 <sup>14</sup>C yr BP were calibrated by matching the obtained conventional AMS <sup>14</sup>C with the calendar ages estimated for MD95-2042 deep-sea core by Bard et al. (2004).

The core was sampled every 5 cm between 2245 cm and 760 cm for microcharcoal and organic carbon content analyses; this interval encompasses the end of MIS 6 to MIS 2.

#### Image analysis for microcharcoal counting

A total of 294 samples were analysed for microcharcoal using automated image analysis in transmitted light. Microcharcoal preparation technique followed the work of Daniou et al. (2007). Chemical treatment was performed over 24 h on 0.2 g of dried sediment and involved the addition of 5 mL of 37% HCl; 5 mL of 68% HNO<sub>3</sub>; 10 mL of 33% H<sub>2</sub>O<sub>2</sub>. This chemical treatment is used to remove pyrites, humic material, labil or less refractory organic matter (OM) and to bleach non-oxidised OM. Dilution of 0.1 was then applied to this residue and this suspension was filtered onto a cellulose acetate membrane containing nitrocellulose of 0.45 μm porosity and 47 mm in diameter. A portion of the membrane was dissolved onto a plexiglass slide with acetate before gentle polishing with alumin powder of 200 μm. The use of polish slide (used classically in petrographic analysis) for image analysis is better than the previously assembling technique consisting of mounting the portion of the membrane onto a slide with Canadian balsam (Daniou et al., 2007) as the focus on the edge of microcharcoal is improved. The slides were scanned with an automated Leica DM6000M microscope at ×500 magnification. In order to have a good statistical representation of each sample, 200 view-fields (200 images) of 0.0614 mm<sup>2</sup> were “grabbed” in color with a 1044×772 pixels digitising camera (1 pixel=0.276 μm). The surface scanned by the microscope represents a surface area of 12.279 mm<sup>2</sup>.

Microcharcoal recognition was performed by using a program of image analysis developed in this study with LeicaQwin software. The subroutine written for microcharcoal identification during image analysis procedure was established by a simultaneous visual identification of microcharcoal in transmitted light following criteria from Boulter (1994), namely black debris, opaque, with sharp edges (see also Enache and Cumming, 2006) and petrographic criteria in reflected light, that is with visible plant structures characterised by thin cell walls and empty cellular

cavities, or particles without plant structure but of similar reflectance than that of previous ones (Noël, 2001). In a controlled light adjustment, a threshold value in red, green, blue (RGB) color was defined to identify microcharcoal based on several observations of particle on different slides.

From measured variables of microcharcoal (surface area, length, width, elongation, number) we calculated for each sample:

- the concentration of microcharcoal (CCnb): number of microcharcoal per gram (nb g<sup>-1</sup>)
- the concentration of microcharcoal surface (CCsurf), which is the sum of all surfaces of microcharcoal in one sample per gram (μm<sup>2</sup> g<sup>-1</sup>). This is to avoid the overrepresentation of microcharcoal concentration as the result of potential fragmentation during production (Théry-Parisot, 1998) or transport.

The three-point running mean “MCCnb” and “MCCsurf” was also calculated for CCnb and CCsurf respectively to be able to compare fire regime with vegetation history of the same core (resolution of 10 cm). The term MCC will be used as global mean average microcharcoal concentration representing microcharcoal concentration variation of number or surface of microcharcoal (as the two microcharcoal concentrations covary, see below).

Replicate analysis was done on 10 samples randomly selected of core MD04-2845, analysed ten times each. Experimental standard deviations were calculated with the equation below. The confidence interval at 95% (see curve in Fig. 3) is derived from the Student's *t*-distribution for *n*–1 degrees of freedom ( $x_i \pm t^*s$  with  $t=2.262$ ).

$$s = \sqrt{\frac{1}{n-1} \sum_{i=1}^n (x_i - \bar{x})^2}$$

The minimum of variation of MCC discussed below is higher than the widen confidence interval so that variations observed in MCC curve are not related to an artefact of sampling bias.

#### Particulate organic carbon (POC) analysis

The organic carbon (OC) content was determined directly on dry weight material sediment by combustion in an LECO CS 200 analyzer (Etcheber et al., 1999) on the same sample depth as that used for microcharcoal analysis. Around 50 mg of powdered and homogenized samples were acidified in crucibles with 2 N HCl to destroy carbonates and then dried at 60°C to remove inorganic carbon and most of the remaining acid and water. The OC analysis was performed by direct combustion in an induction furnace, and the

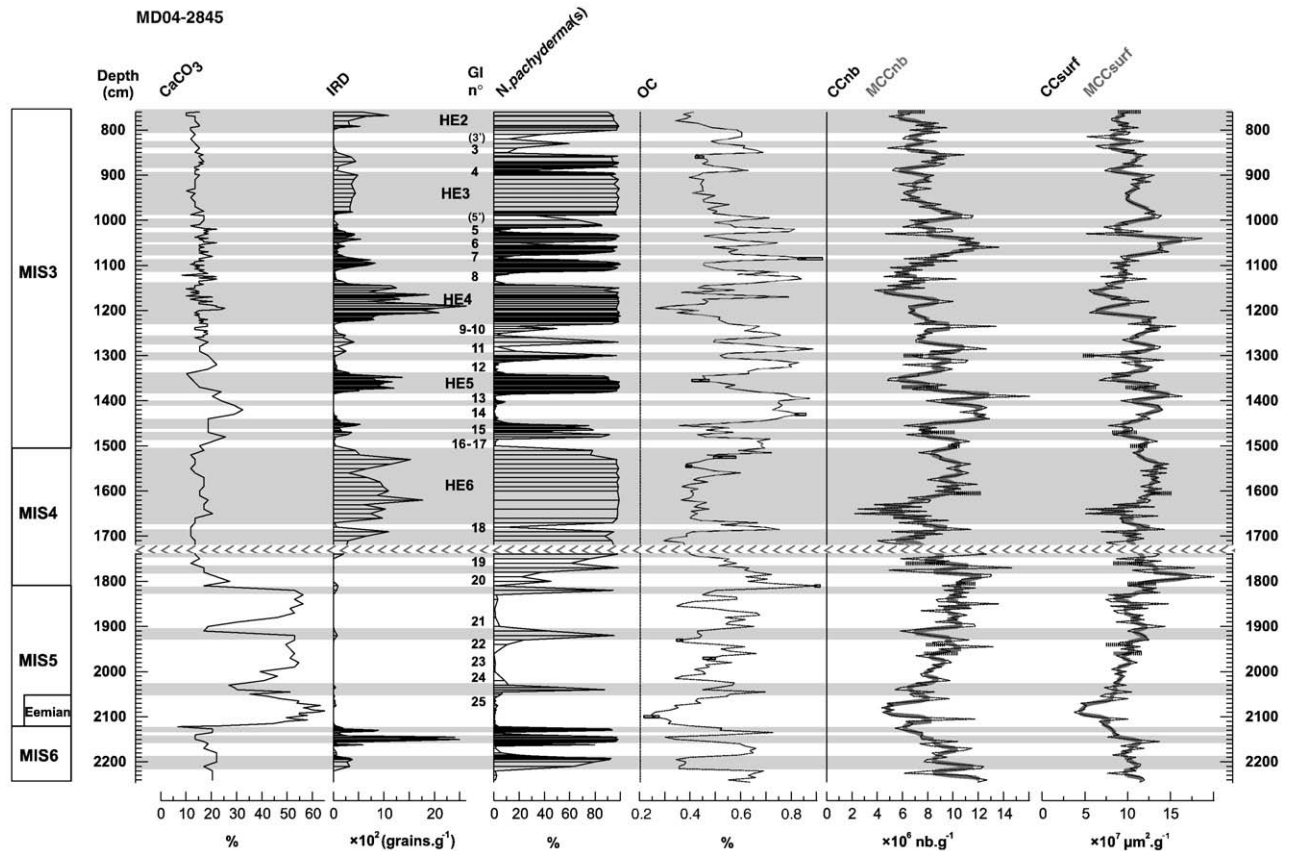


**Figure 3.** Results from microcharcoal and organic carbon content and comparison with other marine proxies of core MD04-2845. All records are plotted versus depth. Limits of Marine Isotopic Stages (MIS) and the Eemian Interglacial are also indicated. From left to right: (a) the carbonate percentages ( $\text{CaCO}_3$ ), (b) the ice rafted debris (IRD) concentration, (c) the polar foraminifera *Neogloboquadrina pachyderma* (s) abundance percentages, (d) the organic carbon content (OC) percentage, (e) the microcharcoal number concentration curve (CCnb) and the three-point running mean (MCCnb), (f) the microcharcoal surface area concentration (CCsurf) and the three-point running mean (MCCsurf). Grey rectangle shown on the OC curve represents the greatest lower and least upper bound of replicates. Dotted bar on microcharcoal concentration curve (CCnb and MCCsurf) indicate the 95% confidence interval. Grey bands indicate Heinrich events and other Dansgaard-Oeschger stadials. Heinrich events are identified on the basis of peaks in ice rafted debris (IRD), high polar foraminifera (*N. pachyderma* s.) percentages and AMS  $^{14}\text{C}$  ages. Greenland interstadial numbers (GI) are also shown. 1714–1740 cm: sedimentary hiatus.

CO<sub>2</sub> formed was determined quantitatively by infrared absorption. Replicate analyses were performed on 10 selected samples reanalysed 6 times each (greatest lower and least upper bound are indicated in Fig. 3).

## Results

### Microcharcoal analysis

Concentration of CCnb varies between  $218.4 \times 10^4$  and  $1607 \times 10^4$  nb  $\text{g}^{-1}$  (Fig. 3). Concentration of CCsurf varies between  $3731 \times 10^4$  and  $20,137 \times 10^4$   $\mu\text{m}^2$   $\text{g}^{-1}$ . CCnb and CCsurf are positively correlated ( $r=0.75$ ;  $R^2=0.56$ ). Visual inspection of MCCnb and MCCsurf reveals high variability superimposed to a long-term trend. A long-term decreasing trend characterises the end of MIS 6 until the middle part of the Eemian, the MIS 4 until the beginning of HE6, and the intervals between GI14–HE4 and GI6–HE2. A long-term trend of increasing values of MCC occurs from the end of the Eemian to the onset of MIS 4.

The high variability of MCCnb and MCCsurf superimposed to the long-term trend shows low values or decreasing values during stadials of MIS 5 and 6 (except GS20), and during GS and HE except for the middle part of HE6 and 4, GS8, GS7, GS4 and GS3. Each of HE are characterised by three phases: a phase of relatively high MCC bracketed by two phases of low MCC. A pronounced decrease of MCC occurs at the end of HE4 and HE3, while HE6 presents a rather

different pattern with a strong decrease of MCC at the beginning of the event.

### Organic carbon (OC)

The OC of core MD04-2845 (Fig. 3) varies between 0.248 and 0.903% (average value of 0.53%) which is comparable to the OC reported in the Bay of Biscay for sediments from the shelf (<0.5%) or deep ocean (average value: 0.5–1%) (Etcheber et al., 1999). The OC values are comparable between the last interglacial (average value of 0.49%) and the LGP (average value of 0.55%). The OC is highly variable for the LGP and parallels the D–O climatic variability with high values during GI and low values during GS and HE. During the last interglacial period, three gradual increases of OC occurred during the Eemian—GS25, GI23–22, GI21 and GI20. The end of MIS 6 presents the same pattern than the LGP with peaks of OC corresponding to interstadials and low values of OC during stadials.

### Time-series analysis

To extract the significant periodicities of our proxies, spectral analysis was applied on linear detrended OC content and microcharcoal concentration (CCsurf and CCnb) before applying the Lomb periodogram algorithm (Past software). Periodicities have been selected for a 0.01 (99%) significance level. Several millennial periodicities are detected in the proxies (see Fig. 4). Most notably,

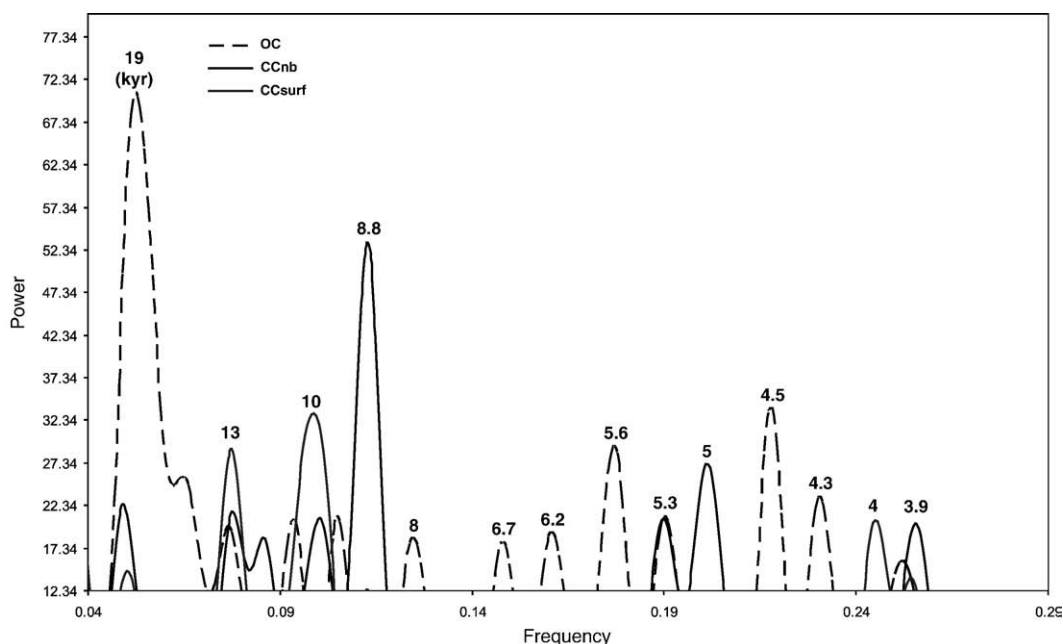


**Figure 4.** Spectral analysis applied to linear detrended OC content and microcharcoal concentration (CCsurf and CCnb) before applying the Lomb periodogram algorithm (Past software). Periodicities (ka) have been selected for a 0.01 (99%) significance level. Peaks in the spectrum are presented with frequency (X-axis) and power value (Y-axis) (units proportional to the square of the amplitudes of the sinusoids present in the data).

341 periods close to the precession (19–20 ka) are detected for OC and  
 342 microcharcoal concentration. CC presents well marked periods of 13,  
 343 10 and 8.8 ka.

#### 344 Discussion

##### 345 Last glacial oceanic circulation and wind direction changes: implications 346 for microcharcoal signal interpretation

347 In order to test whether millennial-scale MCC variation is related  
 348 to actual changes in fire regime and to verify that MCC variation is  
 349 independent of changes in aeolian or fluvial sedimentary input, we  
 350 have used other climatic proxies (pollen, foraminifera derived-SST,  
 351 OC and  $\text{CaCO}_3$ ). OC content parallels the D–O climatic variability with  
 352 an alternation of high and low OC values during GI and GS,  
 353 respectively (Fig. 3). OC content in marine cores is derived  
 354 from marine productivity although a fraction of continental material may  
 355 affect it (Pailler and Bard, 2002). The absence of correlation over the  
 356 record of core MD04-2845 between OC and terrestrial material such  
 357 as microcharcoal and pollen ( $r=0.34$ ,  $p<0.01$  for OC content and  
 358 microcharcoal concentration,  $r=0.16$ ,  $p<0.1$  for OC and pollen  
 359 concentration) implies that such OC variations cannot be explained  
 360 only by changes of continental organic matter supply via wind or  
 361 rivers. Additionally,  $\text{CaCO}_3$  being free of dissolution because of the  
 362 core location above the carbonate compensation depth (Kennett,  
 363 1982), no significant correlation between OC and  $\text{CaCO}_3$  contents ( $r=$   
 364  $-0.13$ ,  $p<0.02$ ) indicates that the OC might derive from non-  
 365 calcifying species such as diatoms or silicoflagellates. Cocolithus  
 366 such as *Emiliana huxelyi*, *Gephyrocapsa* and *Coccolithus pelagicus*,  
 367 which are currently associated with an increase of diatoms and  
 368 silicoflagellates in this region (Beaufort and Heussner, 1999), were  
 369 indeed observed during interstadials in our core (e.g., GI 17–16, J.  
 370 Giraudeau, pers. comm.). This suggests that an increase of OC during  
 371 GI reflects an increase of marine productivity. The OC pattern in core  
 372 MD04-2845 is similar to the pattern of dinoflagellates productivity in  
 373 the marine core MD03-2692 located on the Celtic margin during MIS  
 374 6, where higher concentrations during interstadials and lower ones  
 375 during stadials are observed (Penaud, unpublished data). We there-

fore consider OC to be essentially a proxy of marine productivity in  
 core MD04-2845.

Last glacial productivity changes revealed by a core located off  
 Lisboa were related to variations in Portugal's upwelling system  
 (Pailler and Bard, 2002). However, the Gascogne seamount is far from  
 regions affected today by upwellings in the Bay of Biscay, namely the  
 shelf break or river plumes. This site was also outside the direct  
 influence of upwelling during the LGP because the shelf break was still  
 drowned at the maximum lowstand sea level (maximum of  $\sim 120$  m  
 depth for the last glacial maximum). Therefore, a different mechanism  
 to that explaining the OC content variation in the Iberian margin must  
 be responsible for the observed shifts in OC between GS and GI in our  
 core.

Forest development detected in core MD04-2845 during GI (Fig. 5)  
 suggests an increase of temperatures and precipitation. At present, the  
 increase of humidity as well as river run-off in southwestern France is  
 related with the negative mode of the NAO (Trigo et al., 2002; Dupuis et  
 al., 2006). Climatic conditions in this region during GI might be related,  
 as suggested for southern Iberia (Combourieu Nebout et al., 2002;  
 Moreno et al., 2002; Sánchez Goñi et al., 2002), to a prevailing negative  
 NAO-like situation. Under this climatic regime, SST warming might  
 also be linked to enhanced influence of a warm paleo Navidad current,  
 as occurs today during negative NAO index (García-Soto et al., 2002),  
 favouring productivity blooms and OC increase during the GI. More-  
 over, our hypothesis of the paleo-Navidad current strengthening under  
 a negative NAO-like mode during GI is consistent with the observed  
 weakening of Mediterranean Outflow Water (MOW) at that time  
 (Voelker et al., 2006; Toucanne et al., 2007). The formation of western  
 Mediterranean Deep Water, which likely was a major source of the  
 MOW during the last glacial (Myers et al., 1998; Voelker et al., 2006), is  
 at present positively correlated to the NAO (Rixen et al., 2005).

The comparison between this past oceanic scenario pattern with  
 the modern oceanic and atmospheric circulations (Fig. 2) suggests that  
 GI would be, as in the modern situation, more influenced by  
 southwesterly winds (winter situation) than GS periods that were  
 characterised by prevailing northwesterlies (summer situation). As  
 both wind systems come from the ocean, we do not expect therefore a  
 substantial aeolian contribution of microcharcoal to the Gascogne

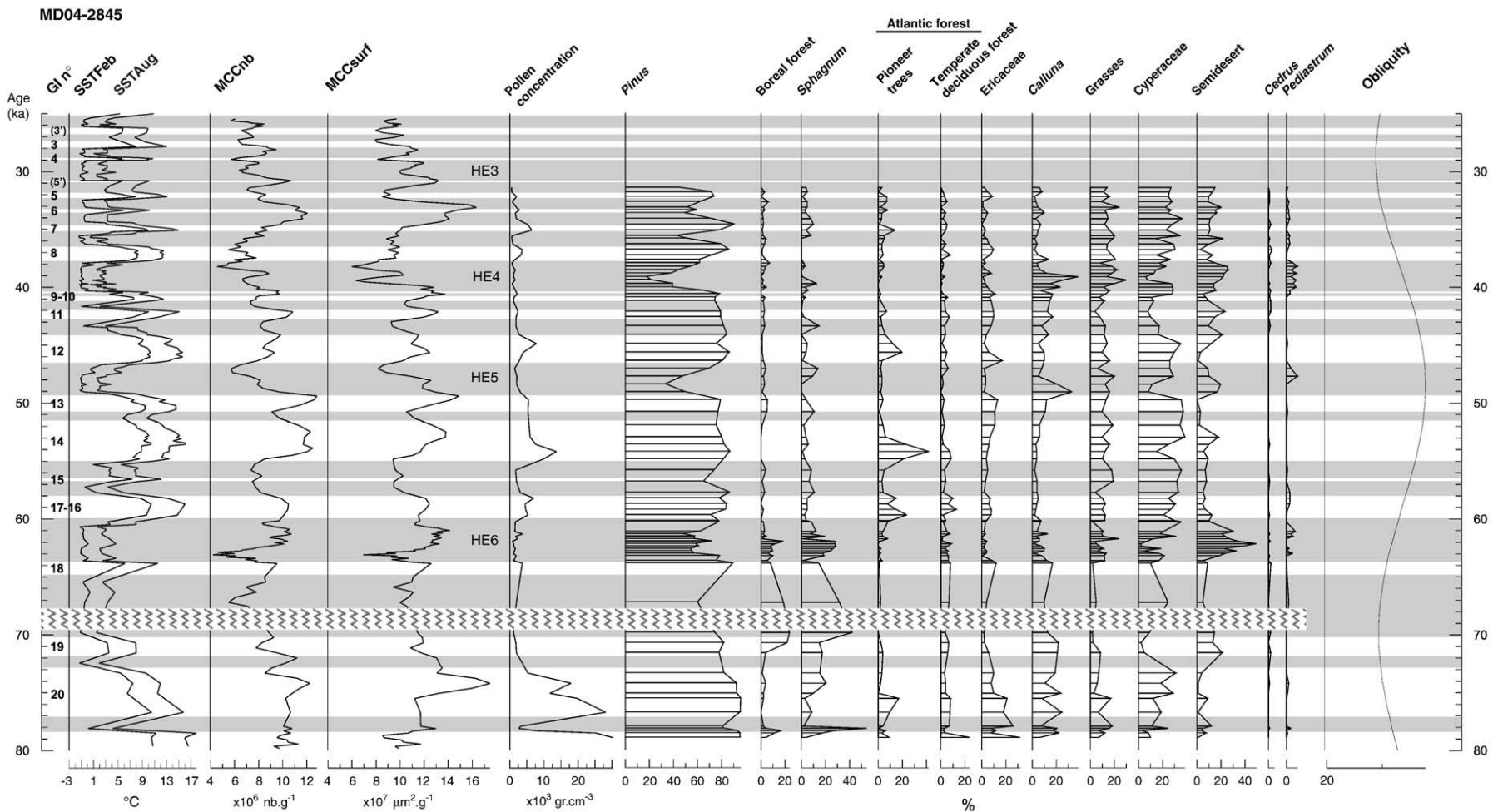


**Figure 5.** Comparison between microcharcoal trends and climatic proxies from core MD04-2845. All records are plotted versus age. From left to right: (a) sea surface temperature derived from foraminifera assemblages for February (SSTFeb) and August (SSTAUG), (b) three-point running mean microcharcoal number concentration curve (MCCnb), (c) three point-running mean microcharcoal surface area concentration curve (MCCsurf), (d) pollen concentration, (e) to (p) pollen group percentage curves, (q) obliquity curve from Laskar et al. (2004). Boreal forest: at 90% *Picea*, *Alnus* and *Salix*; pioneer trees: mainly *Betula*, Cupressaceae and *Hippophæ*; temperate deciduous forest: deciduous *Quercus*, *Carpinus* and *Corylus*; grasses: *Poaceae*; semi-desert: Chenopodiaceae, *Ephedra* and *Artemisia*. Although *Betula* can also belong to boreal forest, percentage variation in our record does not follow the *Picea* pattern, which suggests its inclusion in the Atlantic forest. 68–70 ka: sedimentary hiatus.



seamount during the different phases of the LGP. This is also supported by the sporadic presence of the North African wind-pollinated *Cedrus* tree pollen in the record (Fig. 5), which suggests negligible input of charcoal coming from the South. As with other regions in western Europe (Van Huissteden et al., 2001), the Bay of Biscay was likely characterised by prevailing westerlies during the LGP, suggesting that MCC variability is not controlled by changes in wind directions.

MCC variation in core MD04-2845, retrieved at 350 km from the coast and on a seamount, would be only affected by dilution related to the biogenic or terrigenous hemipelagic input or changes in fluvial sedimentary transfer. The lack of correlation between non-carbonate sedimentary fraction (1-CaCO<sub>3</sub>) or carbonates and microcharcoal concentration ( $r = \pm 0.408$  with CCnb, or  $r = \pm 0.21$  with CCsurf ( $p < 0.01$ )) for the LGP suggests that neither biogenic nor terrigenous material dilute microcharcoal concentration and that MCC variation is not related to changes in fluvial discharges.

MCC variation is therefore not related to changes in aeolian or fluvial sedimentary input, implying that changes in MCC represent variation in regional microcharcoal production and, therefore, in fire regime of western France. Intervals of high MCC values identify periods of strong fire regime, while those marked by low values reveal weak fire regime phases.

#### Fire regime, vegetation composition and climate in western France during the last glacial period

Fire regime is highly variable all along the record, especially during the LGP (Fig. 5): low fire regimes are detected during GS and HE and high fire regimes during GI. This strong fire regime variability may reflect climatic changes, namely succession of dry and humid periods, involving shifts in lightning storm position, changes in fire-sensitive species or variations in fuel availability. In addition, variations of fire regime have likely an impact on vegetation succession. In order to discuss short and long-term fire-climate-vegetation relationship we have compared fire regime changes and fluctuations in vegetation cover and composition (Fig. 5). The vegetation of core MD04-2845 shows that *Betula-Pinus*-deciduous *Quercus* forest expanded during GI and steppic plants (*Artemisia*, Poaceae, heaths and sedges) dominated during the cold and dry GS (Sánchez Goñi et al., 2008).

No continuous and well dated pollen terrestrial records identifying the millennial-scale variability are available in western France. Only the multiproxy study of the Cestas soil, located in southwestern France and reliably related with HE2 (Bertran et al., 2008), sheds light on local vegetation environments at low altitudes. These environments are similar to those described from marine pollen record MD04-2845 and mainly composed by steppic plants such as Poaceae, *Helianthemum* and *Artemisia*, sedges associated with local shrub dominated by *Myrica* and *Ericaceae*.

#### Dansgaard-Oeschger interstadials and stadials

Major differences in fire regime in western France between GS (low fire regime) and GI (high fire regime) are not associated with a particular taxon. Increase in fire regime is associated with periods of afforestation corresponding to the establishment of *Betula-Pinus-deciduous Quercus* open forest during GI, and low fire regime with steppic plants during GS. Some increase of fire regime are also associated to certain peaks of *Ericaceae* and *Calluna* on which repeated fires encourage their regeneration (Bradshaw et al., 1997; Mouillot et al., 2002; Calvo et al., 2002). Beyond the influence of the type and density of the vegetation on the fire regime through changes in fire frequency or severity, increase of microcharcoal concentration during periods of afforestation suggests the increase of microcharcoal production related to increase of woody fuel and biomass accumulation during GI as total plant biomass in forested areas is generally higher than open ground formations (Magri, 1994). This increase of

woody fuel during GI indicates an increase of humidity and associated sea and air surface temperature warming as likely the result of a prevailing negative NAO-like index.

Increase of fire regime related to woody fuel availability for the LGP has been already suggested by Daniau et al. (2007) for southwestern Iberia and inferred from the strong correlation between MCC and forest percentage curves. This hypothesis is supported by the simulation of Ni et al. (2006) for semi-arid regions where lack of fuel, related to drought, often limits the incidence of fire. Although the relationship between fire regime and fuel changes occurs also in western France during the LGP, the tight correlation found in Iberia is less evident in western France. This suggests that in addition to fuel, a direct climatic control may have operated on the fire regime variability of the latter region during the LGP. The reason may be that D-O climatic variability has a lesser impact on vegetation shift between GS and GI which allows the development of a mosaic of vegetation with a dominance of grasses through both GS and GI. At present, a sharp contrast of precipitable water exists in Iberia between negative NAO (high precipitation) and positive NAO (marked drought) situations. Although the same pattern occurs in southwestern France, the contrast of precipitable water is less marked in this region (Trigo et al., 2002). Sánchez Goñi et al. (2008) show that the boundary of the Mediterranean region was similar to that of the present-day during GI. This would imply that a similar gradient of precipitable water than that observed at present-day between the two regions may occur during GI and suggests that during GS (positive NAO-like situation), moisture content in western France is sufficient to develop a continuous vegetation cover, mainly grasses, while lack of winter moisture in southwestern Iberia triggered the development of semi-desert vegetation.

#### Zooming in on Heinrich events 6, 5 and 4

The vegetation of HE 6, 5 and 4 (Fig. 6), mainly composed of *Pinus* woodlands, some *Picea* (well developed during HE6), *Sphagnum*, *Calluna*, and *Cyperaceae* species, is typical of present-day Boreal or central European vegetation, characterised by evergreen coniferous forest and mires which indicate high rainfall areas (Polunin and Walters, 1985). The relative high percentages of *Artemisia* during HE indicates this species occupies drier soils.

**Heinrich event 4.** Fire regime during HE4 presents a three-phase structure (Fig. 6a). Decrease of fire regime at the beginning of HE4, phase (a), is contemporaneous with a large reduction by ~50% of *Pinus* percentages contemporaneous with the succession of *Cyperaceae*, *Sphagnum* and *Calluna* progressively dominating the pollen assemblage. Succession of *Cyperaceae* and *Sphagnum* indicates progressive colonisation of water-filled depressions by fens (minerotrophic peatland) then by bogs (ombrotrophic), which is the typical ecological succession of peatland (mire) (McNamara et al., 1992). This plant succession suggests also a vegetation of transitional mire which forms a mosaic of bog and fen, or occurs where bog and fen succeed each other (Polunin and Walters, 1985). Whereas the development of *Sphagnum* indicates moist or waterlogged environments, this species colonises the upper part of the water table (Rochefort et al., 2002). Most *Sphagnum* species are absent or poorly represented in habitats with an extremely fluctuating water table compared to *Calluna vulgaris* which prefers considerable fluctuations (Laitinen et al., 2007).

The progressive dominance of *Calluna* at the end of this phase and the disappearance of *Sphagnum* suggests an increase of the water table and surface runoff produced by higher precipitation. Even if summer convective rain would promote fire ignitions, relative strong moist conditions would have slowed down fire propagation, leading to the decrease of fire regime during the first phase of HE4, particular in a low fuel availability environment. Increase of fire regime period, phase (b), starts with the beginning of *Pinus* forest development associated with the decline of *Calluna* and the weak

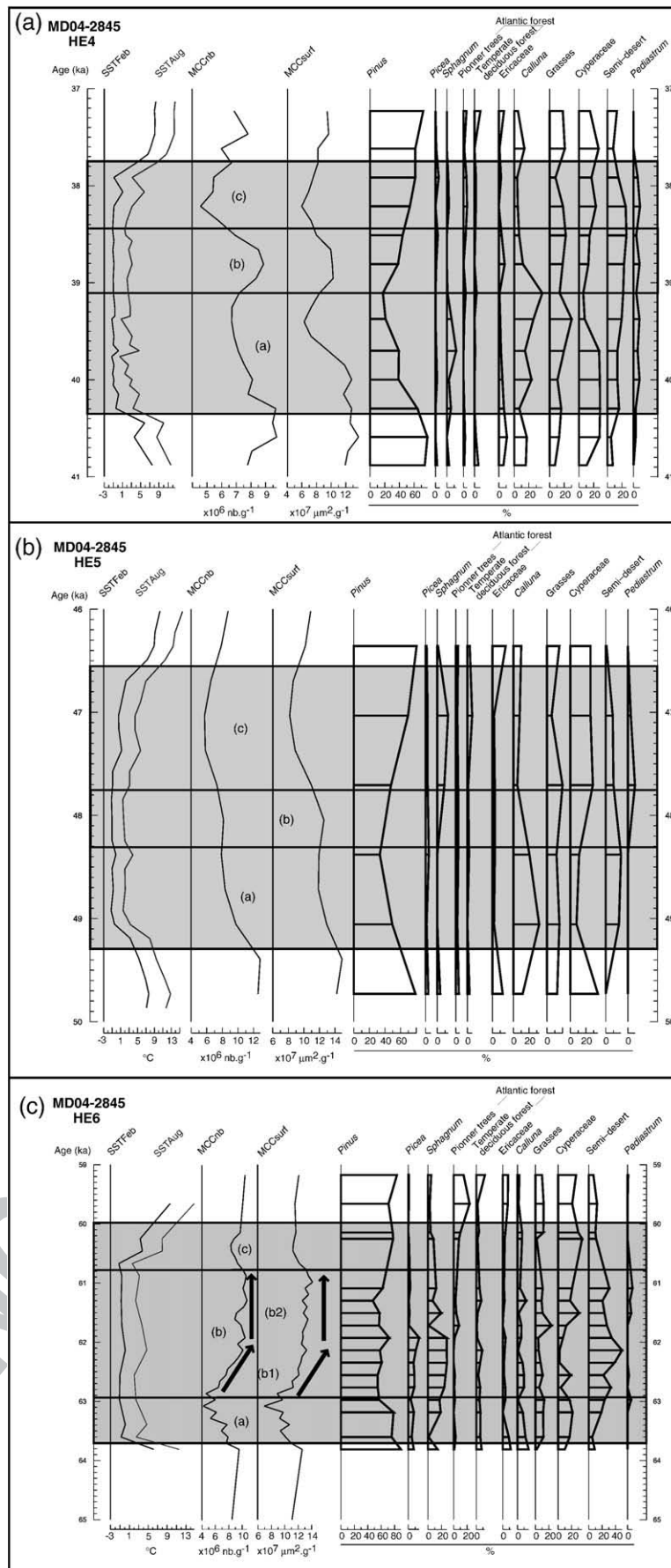


**Figure 6.** Comparison between microcharcoal concentration and climatic proxies during Heinrich events (HE). (a) HE4, (b) HE5, (c) HE6. All records are plotted versus age. (a) Sea surface temperature of February (SSTFeb) and August (SSTAUG), (b) three-point running mean

development of other Ericaceae and semi-desert vegetation. This increase of fire regime contemporaneous with increasing fuel and a decrease of summer precipitation inferred from the decrease of *Calluna* would reflect environmental conditions favourable to fire propagation.

The decrease of fire regime in phase (c) at the end of HE4 is, at first sight, paradoxically associated with the development of mixed-wood forest (*Pinus*, *Picea* and Atlantic forests). The dominance of Cyperaceae and the new development of *Sphagnum* suggest again the development of mire. Although fire regime is expected to increase during this period as woody fuel is available, this wet environment might not promote fire spread, except at the very end of HE4 when *Picea* forest was more developed.

**Heinrich event 5.** As for HE4, three phases in the fire regime characterised HE5 (Fig. 6b). The decrease of fire regime in phase (a) occurs during a humid phase of low woody fuel (*Pinus* forest decline and *Calluna*-dominant vegetation). The relative low resolution of the pollen record during phase (b) precludes discussing the relationship between the increase of fire regime revealed by MCC and changes in forest cover and composition. The hypothesis of environmental conditions similar to HE4's phase (b) controlling this fire regime enhancement needs to be confirmed by higher resolution pollen analysis. The low fire regime in phase (c) is contemporaneous with *Pinus* forest and mire expansions. The record of *Pediastrum* at the very beginning of this phase suggests relative high amount of precipitation or strong snow melting favouring the development of water-filled depressions (lakes, ponds) or lowland rivers (Batten, 1996) during this time. The following succession of Cyperaceae and *Sphagnum* suggests the progressive colonisation of these water-filled depressions.

During HE4 and 5, the progressive increase of annual SST recorded in phase (c) contemporaneous with the development of *Pinus* forest suggests warmer conditions than that of previous phases. Further, *Pinus* forest development during the middle and the last phases of HE4 and 5 would be indicative of a transition from a wet and/or cold (phase (a)) to a dry and/or warm climate (phase (b–c)) inferred from the establishment of trees on peatlands (see a synthesis in Linderholm and Leine, 2004). This drying and warming trend, observed during these two Heinrich events, has been also reported for the western Iberian margin and adjacent landmasses during the last phase of HE1, 2 and 4 (Naughton et al., 2007). In western France, the drying trend during the middle and last phase of HE 4 and 5 would lead to reduce fen landscapes and develop bog-dominated mire. Despite the relative drying and fuel availability, which would favour the increase of fire regime, moisture conditions are assumed to remain important enough in western France to limit propagation of fire at the end of these events. Finally, the increase of fire regime during phase (b), initially attributed to drought, could be also the result of an increase of frequency of lightning storms during this period, which could occur during an atmospheric reorganisation between phases (a) and (c).

**Heinrich event 6.** During HE6, we observe the development of *Picea* forest associated to the expansion of *Sphagnum* and *Pinus* populations, along with *Calluna* and Cyperaceae species, typical of the present-day vegetation of the Boreal region. Interestingly, HE6 is marked by a different vegetation pattern compared to HE5 and 4 because of the relative high percentages of *Pinus* over the entire event and the two slight declines of this tree. However, fire regime is also characterised by a three-phase structure (Fig. 6c). The first low fire regime, phase (a), is associated with *Pinus* forest decline. Phase (b) is characterised by a first strong increase of fire regime (b1) followed by a "plateau" (b2) which coincides with a relatively well developed *Pinus* and *Picea* forest associated with the expansion of *Sphagnum* growing in humid environments and semi-desert plants growing apart in drier soils. The decrease of fire regime at the end of HE6 (c) is associated with the

maximum expansion of Cyperaceae and surprisingly with *Pinus* development.

As for HE4 and 5, the low fire regime during the first and last phases may be related to low fuel content and relative moist conditions limiting fire ignition and spread, respectively. The high fire regime during (b1) may be explained by the development of highly fire sensitive Boreal forest system (Bergeron et al., 2004) associated with particularly dry climate as indicated by the strong development of semi-desert vegetation.

Beyond climatic conditions favourable to *Picea* and *Sphagnum* establishment during this period, high fire regime may have also contributed to the resulting vegetation assemblage. Permafrost forms in peatlands when mean annual temperature (MAT) is below 0°C and becomes continuous when MAT is under -6°C. However, Camill (2000) reports permafrost formation in Canadian boreal peatlands related to dense *Picea mariana* trees and *Sphagnum* dry peat, suggesting that cold temperature is not the unique factor involved in permafrost formation. Alternation between *Picea* and *Sphagnum* species in this region is triggered by fire. *Picea* trees diminish the solar radiation at the surface soil and permafrost begins to form. Fire alters *Picea* forest, the permafrost layer begins to melt and *Sphagnum* develops due to unfrozen conditions. Over time, peat accumulates and succession leads to favourable conditions for tree colonisation, which may promote permafrost formation.

We assume as a working hypothesis that *Picea* and *Sphagnum* grew together in western France during HE6. If we apply the present-day model of *P. mariana* in North America to *Picea* in western Europe, at longer time scale, the development of *Picea-Sphagnum* association during (b1) concomitant with high fire regime suggests that discontinuous permafrost occurred in western France during the transition MIS 4/MIS 3. Moreover, forest fires of this period were probably intense because the expansion of *Sphagnum* populations is favoured by high-temperature forest fires (Greisman, 2006). Paleosols testifying to short occurrence of permafrost have been detected in this region during the youngest HE2 and 1 (Bertran et al., 2008). In addition, evidence of permafrost formation during the HE6 time interval is suggested from growth cessation of the Grotte de Villars's speleothem located in southwestern France (Genty et al., 2003).

Fire regime stays at a high level during (b2) although this period is contemporaneous with woody fuel decrease (*Pinus* and *Picea* population decline) and increase in humidity (*Pediastrum* and Cyperaceae increase). However, *Pinus* forest decline was smaller than in HE4 and 5. At the same time, *Betula* forest-steppe expanded at the expenses of *Picea* (Fig. 5). This environmental succession might indicate thawing of permafrost under the onset of particular warming and drying trend, similar to that reported by Blyakharchuk and Sulerzhitsky (1999) for the western Siberia forest zone during the Holocene. This particular warming coincides with the start of obliquity increase (Fig. 5) and, therefore, enhancement of seasonal contrast at northern latitudes traced in our record by several well-marked GI characterised by the highest development of *Betula* associated with summer SST above 15°C. This particular warming could explain the maintenance of strong fire regime during (b2) likely resulted from particularly high summer temperatures, despite of the decline of *Pinus* and *Picea* forest.

## Conclusion

Microcharcoal and organic carbon analyses were applied to deep-sea core MD04-2845 recovered in the Bay of Biscay, at 45°N. Marine productivity variability revealed by organic carbon content parallels D-O climatic variability and is interpreted as a proxy of paleo-NAO current strength. This current appears to have been reinforced during GI as the result of the prevailing negative NAO-like mode, and inversely during GS. Both GI and GS climatic situations were marked by dominant westerlies and microcharcoal concentration variation is independent of changes in fluvial sedimentary input implying that D-

669 O microcharcoal concentration variability reflects fire regime variation  
670 in western France during the last glacial period.

671 The highest fire regimes are observed during GI related to high-  
672 fuel coniferous-mixed wooded vegetation. Decreasing fire regime is  
673 associated to fuel reduction in a steppe dominated environment  
674 during HE and the other GS. This fire regime pattern is similar to that  
675 observed in southwestern Iberia for the same time period and  
676 supports a regional climatic control of fire regime, through biomass  
677 changes, in western Europe.

678 Contrary to the continuous low fire regime during HE in south-  
679 western Iberia (Daniau et al., 2007), a three-phase structure  
680 characterises fire regime within HE6, 5 and 4 in western France. The  
681 highest fire regime episode is bracketed by two low fire regime  
682 phases. The first low fire regime phase is related to the *Pinus* forest  
683 decline and wet conditions, while the fire increase is contempora-  
684 neous with an afforestation. The late fire decrease is, paradoxically,  
685 associated with the maintenance of substantial woody fuel and dryer  
686 conditions than those of the previous phase. We explain this late  
687 decrease as the result of a new phase of mire expansion. This would  
688 indicate climatic conditions sufficiently moist to limit fire spread.  
689 During HE6, the strong relationship between the highest fire regime  
690 and the expansion of *Picea* and *Sphagnum* communities would reflect  
691 the formation of discontinuous permafrost.

## Q2692 Uncited reference

693 [Komarek et al., 1973](#)

## 694 Acknowledgments

695 The work of A.-L. D. was supported by a BDI CNRS-région Aquitaine  
696 fellowship. This study was funded by the RESOLuTION (ESF-EURO-  
697 CORES-EUROCLIMATE) and ARTEMIS projects. We gratefully acknowl-  
698 edge A. Landouar (Leica Microsystems) who provided useful assistance  
699 for LeicaQwin software language programming, B. Martin and E.  
700 Gonthier for advices and providing access to the slide polishing  
701 machine, H. Etcheber, H. Derriennic and A. Coynel for their introduc-  
702 tion to organic carbon analysis, O. Ther for carbonate measurements,  
703 and J. Giraudeau for looking at the coccoliths of some slides of core  
704 MD04-2845. We also thank W. Fletcher, F. Naughton, S. Toucanne, C.  
705 Lopez-Martinez, J.-M. Jouanneau, P. Bertran, C. Garcia-Soto and S.  
706 Harrison for their valuable comments on different sections of this  
707 manuscript. We also thank 2 anonymous reviewers and Boris  
708 Vannièrre as well as the editor for their valuable comments. This is  
709 Bordeaux 1 University, UMR-CNRS 5805 EPOC Contribution n. 1726.

## 710 References

- 711 Allen, G.P., Castaing, P., 1977. Carte de répartition des sédiments superficiels sur le  
712 plateau continental du Golfe de Gascogne. Bull. Inst. Géol. Bassin d'Aquitaine 21,  
713 255–261.
- 714 Andrae, M.O., Merlet, P., 2001. Emission of trace gases and aerosols from biomass  
715 burning. Global Biogeochemical Cycles 15, 955–966.
- 716 Bard, E., Rostek, F., Ménot-Combes, G., 2004. Radiocarbon calibration beyond 20,000  
717 14C B.P. by means of planktonic foraminifera of the Iberian Margin. Quaternary  
718 Research 61, 204–214.
- 719 Batten, D.J., 1996. Palynofacies and palaeoenvironmental interpretation. In: Jansoni-  
720 us, J., McGregor, D.C. (Eds.), Palynology: Principles and Applications, 3. American  
721 Association of Stratigraphic Palynologists Foundation, pp. 1011–1064.
- 722 Beaufort, L., Heussner, S., 1999. Coccolithophorids on the continental slope of the Bay of  
723 Biscay – production, transport and contribution to mass fluxes. Deep-Sea Research  
724 II 46, 2147–2174.
- 725 Bergeron, Y., Gauthier, S., Flannigan, M., Kafka, V., 2004. Fire regimes at the transition  
726 between mixedwood and coniferous boreal forest in northwestern Quebec. Ecology  
727 85, 1916–1932.
- 728 Bertran, P., Allenet, G., Gé, T., Naughton, F., Poirier, P., Sanchez Goni, M.F., 2008.  
729 Coversand and Pleistocene palaeosols in the Landes region, southwestern France.  
730 Journal of Quaternary Science, doi:10.1002/jqs.1220.
- 731 Blyakharchuk, T.A., Sulerzhitsky, L.D., 1999. Holocene vegetational and climatic changes  
732 in the forest zone of Western Siberia according to pollen records from the  
733 extrazonal palsa bog Bugristoye. The Holocene 9 (5), 621–628.

- Boulter, M.C., 1994. An approach to a standard terminology for palynodebris. In: 734  
735 Traverse, A. (Ed.), Sedimentation of Organic Particles. Cambridge University Press,  
736 Cambridge, pp. 199–216.
- 737 Bradshaw, R.H.W., Tolonen, K., Tolonen, M., 1997. Holocene records of fire from the  
738 boreal and temperate zones of Europe. In: Clark, J.S., Cachier, H., Goldammer, H.,  
739 Stocks, B. (Eds.), Sediment Records of Biomass Burning and Global Change. 739  
740 Springer-Verlag, Berlin, pp. 347–365.
- 741 Calvo, L., Tarrega, R., Luis, E., 2002. Regeneration patterns in a *Calluna vulgaris* heathland  
742 in the Cantabrian mountains (NW Spain): effect of burning, cutting and ploughing. 742  
743 Acta Oecologia 23, 81–90.
- 744 Camill, P., 2000. How much do local factors matter for predicting transient ecosystem  
745 dynamics? Suggestions from permafrost formation in boreal peatlands. Global  
746 Change Biology 6, 169–182.
- 747 Castaing, P., 1981. Le transfert à l'océan des suspensions estuariennes. Cas de la Gironde.  
748 Doct. es Sciences thesis, Université Bordeaux1.
- 749 Colas, F., 2003. Circulation et dispersion lagrangiennes en Atlantique Nord-Est. Thesis,  
750 Université de Bretagne Occidentale.
- 751 Combourieu Nebout, N., Turon, J.L., Zahn, R., Capotondi, L., Londeix, L., Pahnke, K., 2002.  
752 Enhanced aridity and atmospheric high-pressure stability over the western  
753 Mediterranean during the North Atlantic cold events of the past 50 ky. Geological  
754 Society of America 30, 863–866.
- 755 Crutzen, P.J., Heidt, L.E., Krasnec, J.P., Pollock, W.H., Seiler, W., 1979. Biomass burning as a  
756 source of atmospheric gases CO, H<sub>2</sub>, N<sub>2</sub>O, NO, CH<sub>3</sub>Cl and COS. Nature 282, 253–256.
- 757 Daniau, A.L., Sánchez Goni, M.F., Beaufort, L., Laggon-Dégarre, F., Loutre, M.F., Duprat, J.,  
758 2007. Dansgaard-Oeschger climatic variability revealed by fire emissions in  
759 southwestern Iberia. Quaternary Science Reviews 26, 1369–1383.
- 760 Dupuis, H., Michel, D., Sottolichio, A., 2006. Wave climate evolution in the Bay of Biscay  
761 over two decades. Journal of Marine Systems 63, 105–114.
- 762 Durrieu de Madron, X., Castaing, P., Nyffeler, F., Coup, T., 1999. Slope transport of  
763 suspended particulate matter on the Aquitanian margin of the Bay of Biscay. Deep-  
764 Sea Research II 46, 2003–2027.
- 765 Enache, M.D., Cumming, B.F., 2006. Tracking recorded fires using charcoal morphology  
766 from the sedimentary sequence of Prosser Lake, British Columbia (Canada). 766  
767 Quaternary Research 65, 282–292.
- 768 European Commission, 2001. Forest Fires In Southern Europe. Environment and Geo-  
769 Information Unit report 1 (July).
- 770 Etcheber, H., Relexans, J.C., Beliard, M., Weber, O., Buscail, R., Heussner, S., 1999.  
771 Distribution and quality of sedimentary organic matter on the Aquitanian margin  
772 (Bay of Biscay). Deep-Sea Research II 46, 2249–2288.
- 773 Flückiger, J., Blunier, T., Stauffer, B., Chappellaz, J., Spahni, R., Kawamura, K., Schwander,  
774 J., Stocker, T.F., Dahl-Jensen, D., 2004. N<sub>2</sub>O and CH<sub>4</sub> variations during the last glacial  
775 epoch: insight into global processes. Global Biogeochemical Cycles 18, 775
- 776 Froidefond, J.M., Castaing, P., Jouanneau, J.M., 1996. Distribution of suspended matter in  
777 a coastal upwelling area. Satellite data and in situ measurements. Journal of Marine  
778 Systems 8, 91–105.
- 779 Garcia-Soto, C., Pingree, R.D., Valdes, L., 2002. Navidad development in the southern Bay  
780 of Biscay: climate change and swoddy structure from remote sensing and in situ  
781 measurements. Journal of Geophysical Research 107 (C8), 3118.
- 782 Genty, D., Blamart, D., Ouahdi, R., Gilmour, M., Baker, A., Jouzel, J., Van-Exter, S., 2003.  
783 Precise dating of Dansgaard-Oeschger climate oscillations in western Europe from  
784 stalagmite data. Letters to Nature 421.
- 785 Greisman, A., 2006. Fire, forest and cultural landscape history during the last  
786 11,000 years in Småland – a case study at Stavsåkra. ESS Bulletin 4, 786
- 787 Heaps, N.S., 1980. A mechanism for local upwelling along the European continental  
788 slope. Oceanologica Acta 3, 449–454.
- 789 Hu, F.S., Brubaker, L.B., Gavin, D.G., Higuera, P.E., Lynch, J.A., Rupp, T.S., Tinner, W., 2006.  
790 How climate and vegetation influence the fire regime of the Alaskan boreal biome:  
791 the Holocene perspective. Mitigation and Adaptation Strategies for Global Change  
792 11, 829–846C, doi:10.1007/s11027-005-9015-4. 792
- 793 Hughen, K.A., Baillie, M.G.L., Bard, E., Bayliss, A., Beck, J.W., Bertrand, C., Blackwell, P.G.,  
794 Buck, C.E., Burr, G., Cutler, K.B., Damon, P.E., Edwards, R.L., Fairbanks, R.G., Friedrich,  
795 M., Guilderson, T.P., Kromer, B., McCormac, F.G., Manning, S., Bronk Ramsey, C.,  
796 Reimer, P.J., Reimer, R.W., Remmele, S., Southon, J.R., Stuiver, M., Talamo, S., Taylor,  
797 F.W., van der Plicht, J., Weyhenmeyer, C.E., 2004. Marine04 marine radiocarbon age  
798 calibration, 0–26 cal kyr BP. Radiocarbon 46, 1059–1086. 798
- 799 Jouanneau, J.M., Weber, O., Cremer, M., Castaing, P., 1999. Fine-grained sediment budget  
800 on the continental margin of the Bay of Biscay. Deep-Sea Research II 46, 2205–2220.
- 801 Kennett, J.P., 1982. Marine Geology. Prentice-Hall, Englewood Cliffs, New Jersey. 801
- 802 Komarek, E.V., Komarek, B.B., Carlyle, C., 1973. The Ecology of Smoke Particulates and  
803 Charcoal Residues from Forest and Grassland Fires: a Preliminary Atlas. Tall Timbers  
804 Research Station, Tallahassee, Florida, p. 75. 804
- 805 Koutsikopoulos, C., le Cann, B., 1996. Physical processes and hydrological structures  
806 related to the Bay of Biscay anchovy. Scientia Marina 60 (2), 9–19. 806
- 807 Laitinen, J., Rehell, S., Oksanen, J., 2007. Community and species responses to water level  
808 fluctuations with reference to soil layers in different habitats of mid-boreal mire  
809 complexes. Plant Ecology, doi:10.1007/s11258-007-9271-3. 809
- 810 Laskar, J., Robutel, P., Joutel, F., Gastineau, M., Correia, A., Levrard, B., 2004. A long term  
811 numerical solution for the insolation quantities of the Earth. Astronomy and  
812 Astrophysics 428, 261–285. 812
- 813 Lazure, P., Jégou, A.M., 1998. 3D modelling of seasonal evolution of Loire and Gironde  
814 plumes on Biscay Bay continental shelf. Oceanologica Acta 21, 165–177. 814
- 815 Lericolais, G., Berné, S., Féliens, H., 2001. Seaward pinching out and internal stratigraphy of  
816 the Gironde incised valley on the shelf (Bay of Biscay). Marine Geology 175, 183–197. 816
- 817 Linderholm, H.W., Leine, M., 2004. An Assessment of twentieth century tree-cover  
818 changes on a southern Swedish peatland combining dendrochronology and aerial  
819 photograph analysis. Wetlands 24, 357–363. 819

- 820 Lobert, J.M., Scharffe, D.H., Hao, W.M., Crutzen, P.J., 1990. Importance of biomass  
821 burning in the atmospheric budgets of nitrogen-containing gases. *Nature* 346,  
822 552–554.
- 823 Magri, D., 1994. Late-Quaternary changes of plant biomass as recorded by pollen-  
824 stratigraphical data: a discussion of the problem at Valle di Castiglione, Italy.  
825 *Review of Palaeobotany and Palynology* 81, 313–325.
- 826 McNamara, J.P., Siegel, D.I., Glaser, P.H., Beck, R.M., 1992. Hydrogeologic controls on  
827 peatland development in the Malloryville Wetland, New York (USA). *Journal of*  
828 *Hydrology* 140, 279–296.
- 829 Moreno, A., Cacho, I., Canals, M., Prins, M., Sánchez Goñi, M.F., Grimalt, J.O., Weltje, G.J.,  
830 2002. Saharan dust transport and high-latitude glacial climate variability: the  
831 Alboran sea record. *Quaternary Research* 58, 318–328.
- 832 Mouillot, F., Rambal, S., Joffre, R., 2002. Simulating climate change impacts on fire  
833 frequency and vegetation dynamics in a Mediterranean-type ecosystem. *Global*  
834 *Change Biology* 8, 423–437.
- 835 Myers, P.G., Haines, K., Rohling, E.J., 1998. Modeling the paleocirculation of the  
836 Mediterranean: the last glacial maximum and the Holocene with emphasis on the  
837 formation of sapropel S1. *Paleoceanography* 13, 586–606.
- 838 Naughton, F., Sánchez Goñi, M.F., Desprat, S., Turon, J.-L., Duprat, J., Malaizé, B., Joli,  
839 C., Cortijo, E., Drago, T., Freitas, M.C., 2007. Present-day and past (last  
840 25000 years) marine pollen signal off western Iberia. *Marine Micropaleontology*  
841 62, 91–114.
- 842 Ni, J., Harrison, S.P., Prentice, I.C., Kutzbach, J.E., Sitch, S., 2006. Impact of climate  
843 variability on present and Holocene vegetation: a model-based study. *Ecological*  
844 *Modelling* 191, 469–486.
- 845 Noël, H., 2001. Caractérisation et calibration des flux organiques sédimentaires dérivant  
846 du bassin versant et de la production aquatique (Annecy, le Petit lac). Rôles  
847 respectifs de l'Homme et du climat sur l'évolution des flux organiques au cours des  
848 6000 dernières années. Ph. D. Thesis, Sciences de l'Univers, Pétrographie et  
849 Géochimie Organiques, Université d'Orléans, Orléans, France.
- 850 Ozenda, P., 1982. *Les Végétaux Dans La Biosphère*. Paris, Doin, p. 431.
- 851 Pailler, D., Bard, E., 2002. High frequency palaeoceanographic changes during the past  
852 140,000 yr recorded by the organic matter in sediments of the Iberian margin.  
853 *Palaeogeography, Palaeoclimatology, Palaeoecology* 181, 431–452.
- 854 Petit, J.R., Jouzel, J., Raynaud, D., Barkov, N.I., Barnola, J.-M., Basile, I., Bender, M.,  
855 Chappellaz, J., Davis, M., Delaygue, G., Delmotte, M., Kotlyakov, V.M., Legrand, M.,  
856 Lipenkov, V.Y., Lorius, C., Pepin, L., Ritz, C., Saltzman, E., Stievenard, M., 1999. Climate  
857 and atmospheric history of the past 420,000 years from the Vostok ice core,  
858 Antarctica. *Nature* 399, 429–436.
- 859 Polunin, O., Walters, M., 1985. *A Guide to the Vegetation of Britain and Europe*. Oxford  
860 University Press, New York.
- 861 Power, M.J., Marlon, J., Ortiz, N., Bartlein, P.J., Harrison, S.P., Mayle, F.E., Ballouche, A.,  
862 Bradshaw, R.H.W., Carcaillet, C., Cordova, C., Mooney, S., Moreno, P.I., Prentice, I.C.,  
863 Thonicke, K., Tinner, W., Whitlock, C., Zhang, Y., Zhao, Y., Ali, A.A., Anderson, R.S.,  
864 Beer, R., Behling, H., Briles, C., Brown, K.J., Brunelle, A., Bush, M., Camill, P., Chu, G.Q.,  
865 Clark, J., Colombaroli, D., Connor, S., Daniau, A.-L., Daniels, M., Dodson, J., Doughty,  
866 E., Edwards, M.E., Finsinger, W., Foster, D., Frechette, J., Gaillard, M.J., Gavin, D.G.,  
867 Gobet, E., Haberle, S., Hallett, D.J., Higuera, P., Hope, G., Horn, S., Inoue, J.,  
868 Kaltenreider, P., Kennedy, L., Kong, Z.C., Larsen, C., Long, C.J., Lynch, J., Lynch, E.A.,  
869 McGlone, M., Meeks, S., Mensing, S., Meyer, G., Minckley, T., Mohr, J., Nelson, D.M.,  
870 New, J., Newnham, R., Noti, R., Oswald, W., Pierce, J., Richard, P.J.H., Rowe, C.,  
871 Sánchez Goñi, M.F., Shuman, B.J., Takahara, H., Toney, J., Turney, C., Urrego-Sanchez,  
872 D.H., Umbanhowar, C., Vandergoes, M., Vanniere, B., Vescovi, E., Walsh, M., Wang,  
873 X., Williams, N., Wilmshurst, J., Zhang, J.H., 2007. Changes in fire regimes since the  
874 Last Glacial Maximum: an assessment based on a global synthesis and analysis of  
875 charcoal data. *Climate Dynamics*, doi:10.1007/s00382-007-0334-x.
- 876 Puillat, I., Lazure, P., Jégou, A.M., Lampert, L., Miller, P.I., 2004. Hydrographical variability  
877 on the French continental shelf in the Bay of Biscay, during the 1990s. *Continental*  
878 *Shelf Research* 24, 1143–1163.
- Rixen, M., Beckers, J.-M., Levitus, S., Antonov, J., Boyer, T., Maillard, C., Fichaut, M., 879  
Balopoulos, E., Iona, S., Dooley, H., Garcia, M.J., Manca, B., A., G., Manzella, G., 880  
Mikhailov, N., Pinardi, N., Zavatarelli, M., the Medar Consortium, 2005. The Western 881  
Mediterranean Deep Water: a proxy for climate change. *Geophysical Research* 882  
Letters 32 NIL\_47-NIL\_50. 883
- Rochefort, L., Campeau, S., Bugnon, J.-L., 2002. Does prolonged flooding prevent or 884  
enhance regeneration and growth of Sphagnum? *Aquatic Botany* 74, 327–341. 885
- Ruch, P., Mirmand, M., Jouanneau, J.-M., Latouche, C., 1993. Sediment budget and 886  
transfer of suspended sediment from the Gironde estuary to Cap Ferret Canyon. 887  
*Marine Geology* 111, 109–119. 888
- Sánchez Goñi, M.F., Cacho, I., Turon, J.-L., Guiot, J., Sierro, F.J., Peypouquet, J.P., Grimalt, J.O., 889  
Shackleton, N.J., 2002. Synchronicity between marine and terrestrial responses to 890  
millennial scale climatic variability during the last glacial period in the Mediterranean 891  
region. *Climate Dynamics* 19, 95–105. 892
- Sánchez Goñi, M.F., Landais, A., Fletcher, W., Naughton, F., Desprat, S., Duprat, J., 2008. 893  
Contrasting impacts of Dansgaard-Oeschger events over a western European 894  
latitudinal transect modulated by orbital parameters. *Quaternary Science Reviews* 895  
27, 1136–1151. 896
- Serryn, P., 1994. *Atlas Bordas Géographique*. Hölzel, Paris. 897
- Shackleton, N.J., et al., 2000. MD95-2042 Oxygen and Carbon Isotope Data. IGBP PAGES/ 898  
World Data Center A for Paleoclimatology Data Contribution Series #2000-066. 899  
NOAA/NGDC Paleoclimatology Program, Boulder CO, USA. 900
- Shackleton, N.J., Fairbanks, R.G., Chiu, T.-C., Parrenin, F., 2004. Absolute calibration of the 901  
Greenland time scale: implications for Antarctic time scales and for  $\Delta 14C$ . 902  
*Quaternary Science Reviews* 23, 1513–1522. 903
- Stuiver, M., Reimer, P.J., 1993. Extended  $^{14}C$  database and revised CALIB radiocarbon 904  
calibration program. *Radiocarbon* 35, 215–230. 905
- Stuiver, M., Reimer, P.J., Reimer, R.W., 2005. CALIB 5.0. (www program and 906  
documentation). 907
- Théry-Parisot, I., 1998. *Economie du combustible et Paléocologie en contexte glaciaire* 908  
et périglaciaire, Paléolithique moyen et supérieur du sud de la France. *Anthracologie,* 909  
*Experimentation, Taphonomie*. Thesis, Université de Paris I Panthéon- 910  
Sorbonne. 911
- Thonicke, K., Prentice, I.C., Hewitt, C., 2005. Modeling glacial-interglacial changes in 912  
global fire regimes and trace gas emissions. *Global Biogeochemical Cycles* 19, 913  
GB3008, doi:10.1029/2004GB002278. 914
- Toucanne, S., Mulder, T., Schönfeld, J., Hanquiez, V., Gonthier, E., Duprat, J., Cremer, M., 915  
Zaragosi, S., 2007. Contourites of the Gulf of Cadiz: a high-resolution record of the 916  
paleocirculation of the Mediterranean outflow water during the last 50,000 years. 917  
*Palaeogeography, Palaeoclimatology, Palaeoecology* 246, 354–366. 918
- Trigo, R.M., Osborn, T.J., Corte-Real, J.M., 2002. The North Atlantic Oscillation influence 919  
on Europe: climate impacts and associated physical mechanisms. *Climate Research* 920  
20, 9–17. 921
- Turon, J.-L., 1984. Le palynoplanton dans l'environnement actuel de l'Atlantique nord- 922  
oriental. Evolution climatique et hydrologique depuis le dernier maximum 923  
glaciaire. *Mémoires de l'Institut de Géologie du bassin d'Aquitaine* (17) Université 924  
de Bordeaux I, Bordeaux. 925
- van Aardenne, J.A., Dentener, F.J., Oliver, J.G.J., Klein Goldewijk, C.G.M., Lelieveld, J., 2001. 926  
A 1 X 1 resolution data set of historical anthropogenic trace gas emissions for the 927  
period 1890–1990. *Global Biogeochemical Cycles* 15, 909–928. 928
- Van der Werf, G.R., Randerson, J.T., Collatz, G.J., Giglio, L., Kasibhatla, S., Arellano, J.A.F., 929  
Olsen, S.C., Kasischke, E.S., 2004. Continental-scale partitioning of fire emissions 930  
during the 1997 to 2001 El Niño/La Niña Period. *Science* 303, 73–76. 931
- Van Huissteden, J., Gibbard, P.L., Briant, R.M., 2001. Periglacial fluvial systems in 932  
northwest Europe during oxygen isotope stages 4 and 3. *Quaternary International* 933  
79, 75–88. 934
- Voelker, A.H.L., Lebreiro, S.M., Schönfeld, J., Cacho, I., Erlenkeuser, H., Abrantes, F., 2006. 935  
Mediterranean outflow strengthening during northern hemisphere coolings: a salt 936  
source for the glacial Atlantic? *Earth and Planetary Science Letters* 245, 39–55. 937

938

939